In vitro corrosion behavior and cytocompatibility of pure Fe implanted with Ta

Henan Wang[1], Yang Zheng[1], Chengbao Jiang[1], Yan Li[1],* Yongqing Fu[2,**]

[1]School of Materials Science and Engineering, Beihang University, Beijing 100191, China.

[2]Faculty of Engineering and Environment, Northumbria University, Newcastle Upon Tyne NE1 8ST, United Kingdom

Abstract

In this study, pure Fe was surface-modified by Ta ion implantation with different incident ion doses. Its surface morphology and chemical composition were investigated using atomic force microscopy and auger electron spectroscopy. Results showed that Ta ion implantation led to the formation of Ta/Fe oxide mixtures at the outmost surface (60-80 nm in thickness) of the implanted layer. Results from electrochemical measurements and immersion tests indicated that the corrosion rate of the pure Fe in simulated body fluids can be accelerated after the Ta ion implantation. The *in vitro* cell culture results showed that the cytocompatibility of osteoblasts on the pure Fe has been significantly improved by applying the Ta ion implantation.

Keywords: Fe; Ta; Ion implantation; Corrosion; Cytocompatibility

* Corresponding Author: Yan Li, E-mail: liyan@buaa.edu.cn, Tel: +86 10 82315989

**Co-corresponding Author: Richard YongQing Fu, E-mail:Richard.fu@northumbria.ac.uk

1. Introduction

Fe and its alloys have attracted increasing attention to be used as degradable biomedical devices such as cardiovascular stents and orthopedic implants [1-4]. The feasibility of the Fe-based alloys as biodegradable implants has been verified by both *in vitro* and *in vivo* studies [5-8]. The preliminary *in vivo* animal trails indicated that pure Fe showed a good short-term biocompatibility in the porcine aorta and it exhibited similar vessel, inflammatory and healing parameters as those of Co-Cr stents [9]. However, the very slow degradation rate of the Fe-based alloys in physiological environments restricts their wide clinical applications [9, 10].

Ion implantation is an effective technique to enhance the performance of biomedical alloys through adjusting their surface composition and microstructure [11-14]. It is well known that Ta is a good bio-metallic element and has been widely used in biomedical applications [15-17]. Implantation of Ta can significantly improve the proliferation rate of L929 mouse fibroblast-like cells on the surface of NiTi alloy [12]. However, to the best of our knowledge, few studies have been reported on the effects of Ta ion implantation on the corrosion behavior and cytocompatibility of the pure Fe. In the present work, the pure Fe samples were modified by Ta ion implantation and, the effectiveness of Ta on accelerating the corrosion rate and improving the cytocompatibility of the pure Fe were investigated through the analysis of surface characteristics.

2. Materials and methods

2.1 Sample preparation

Commercial pure Fe (99.5%) with the size of 10×10×2 mm^3 was mechanically polished with SiC emery papers and ultrasonically cleaned in acetone. The metal ion implantation equipment

(MEVVA 100) was employed to implant the Ta ions. The Ta ion implantation parameters and the corresponding sample names are listed in Table 1.

Table 1 Ion implantation parameters of Ta implanted Fe (Ta-Fe) samples.

Samples	Fe	Ta-Fe-5	Ta-Fe-10	Ta-Fe-30
Base pressure (Pa)	0	1×10^{-4}	1×10^{-4}	1×10^{-4}
Ion current (mA)	0	2	2	2
Bias voltage (kV)	0	-45	-45	-45
Dose ($\times10^{16}$ ions/cm^2)	0	5	10	30

2.2 Surface characterization

Atomic Force Microscope (AFM, Veeco Instruments, USA) was employed for the observation of 3D topography on the sample surface using the tapping mode. The Auger Electron Spectroscopy (AES, ULVACUPHI, Japan) was utilized to determine the elemental depth profiles using a 5 kV primary electron beam with an analytical rate of 18 nm/min based on the analysis of a reference SiO_2 film.

2.3 *In vitro* degradation tests

Electrochemical measurements in the simulated body fluid (SBF) were performed using an electrochemical workstation (CHI 660e, CH Instruments Inc., Shanghai). The composition of the SBF is 142.0 mM Na^+, 5.0 mM K^+, 1.5 mM Mg^{2+}, 2.5 mM Ca^{2+}, 147.8 mM Cl^-, 4.2 mM HCO_3^-, 1.0 mM HPO_4^{2-} and 0.5 mM SO_4^{2-} with a pH value of 7.40 [18]. In a standard potentiodynamic polarization measurement, the applied potential was increased from cathodic region to anodic region at a scan rate of 1 mV/s after stabilization for 1 hour.

The immersion tests were conducted based on the ASTM standard G31-72 and the ratio of surface area to SBF volume was 1 cm^2/40 mL [19]. The corroded morphology and corrosion products

were analyzed using the Scanning Electron Microscope (SEM,Quanta 200F).

2.5 Direct cell culture

Rat embryo osteoblasts (MC3T3-E1), provide by the Graduate School of Basic Medical Science, China, were used for the evaluation of *in vitro* cytocompatibility. The cells were cultured in α-Modified Eagle's Medium (α-MEM, Gibco, Australia) supplemented with 10% v/v fetal bovine serum (GIBCO, Australia) and antibiotics (100 U/mL of penicillin and 100 mg/mL of streptomycin) at 37 °C and 5% CO_2. The cell suspension with approximate 1×10^4cells were seeded onto each sample surface and cultured for 24 hours. After that, the samples were gently rinsed with Phosphate-Buffered Solution (PBS) and immersed in 2.5% glutaraldehyde for 1 hour. After washing with the PBS, the cells were dehydrated in sequential concentrations of ethanol and further dehydrated in hexamethyldisilizane for 1 hour and then dried in air. The morphologies of the adhered cells were observed using the SEM after treating the samples with platinum spraying.

3. Results and discussion

Three-dimensional topography images from the AFM analysis and average surface roughness (R_a) of the pure Fe and Ta-Fe samples are shown in Fig. 1. From Fig. 1a, the surface of pure Fe, with an R_a value of 8.5±0.4 nm, is seen with many parallel grooves which were generated from the mechanical grinding process. Significant changes of surface morphology and roughness can be observed after the Ta ion implantation with different incident doses. As seen in Fig. 1b, large amounts of island-like nano-protrusions appear on the surface of Ta-Fe-5 sample and its R_a value is increased to 10.7±0.6 nm. It is shown in Fig. 1c that the nano-protrusions become larger as the Ta ion dose is increased. A much rougher surface with an R_a value of 21.7±0.4 nm can be found for the Ta-Fe-10 sample. For the Ta-Fe-30 sample, as shown in Fig. 1d, the protrusions increase to sub-micrometer

scale and are linked together at the largest Ta ion dose, forming a compact and uniform surface with the smallest R_a value of 3.4±0.3 nm. It should be noted that the changes in the surface roughness are influenced by two opposite effects of ion sputtering and growth of nano-protrusions [20]: the R_a value is increased by the sputtering effect of ion implantation under a lower ion dose, whereas it is decreased by the growth of nano-protrusions under a higher ion dose.

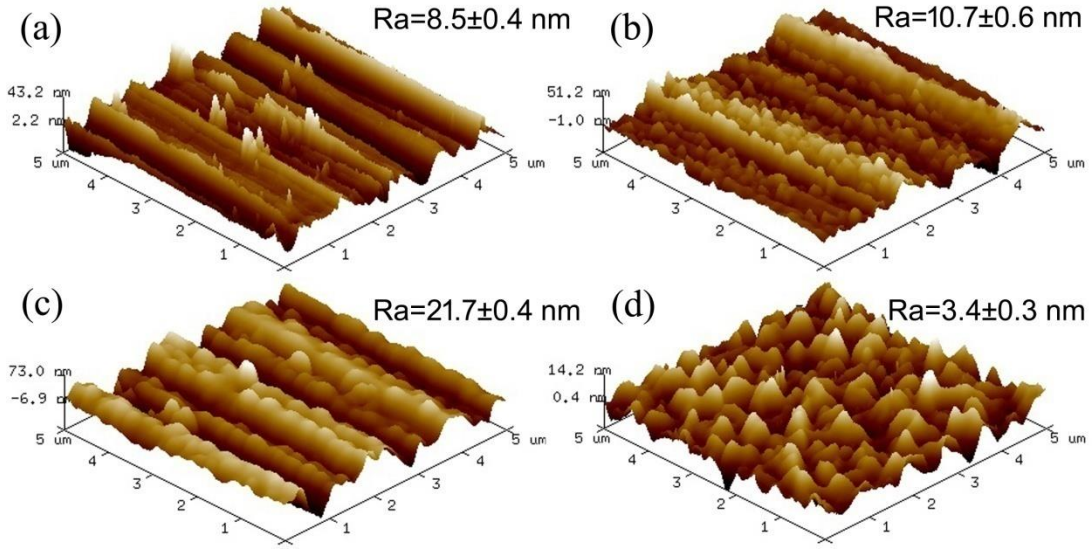

Fig. 1. AFM images and average surface roughness (R_a) values of (a) pure Fe, (b) Ta-Fe-5, (c) Ta-Fe-10 and (d) Ta-Fe-30 samples

Fig. 2 shows the AES depth profiles of Ta, O and Fe elements in the near surface of Ta-Fe samples. As shown in Fig. 2a, the outmost surface of the Ta-Fe-5 sample is mainly composed of 61.2% Fe and 37.5% O with a trace amount of 1.3% Ta. As the depth is increased to 7 nm, the Fe concentration increases linearly to around 90%, while the O concentration decreases sharply to near 4%. In the depth from 7 to 60 nm, the implanted Ta approximately forms a Gaussian distribution with a peak concentration of 12.7% at a depth of 30 nm and simultaneously the Fe concentration shows a reverse trend. The O concentration remains as low as 2.5% within the same depth range. Only Fe element can be detected as the sputtering depth is increased over 60 nm (i.e., reaching the substrate).

Similar elemental distributions can be observed for the Ta-Fe-10 and Ta-Fe-30 samples. It is seen from Fig. 2b that the modified layer of the Ta-Fe-10 sample is about 70 nm with a maximum Ta concentration of 18.2%. A thicker modified layer of ~80 nm and a higher maximum Ta concentration of 22.4% can be detected for the Ta-Fe-30 sample as shown in Fig. 2c. It can be concluded that the modified layer thickness increases from 60 to 80 nm with increasing the Ta ion dose and mixtures of the Ta/Fe oxides are formed on the outmost surface of the Ta-Fe samples. It is suggested that the Ta/Fe oxides on the surface were caused by the reaction of oxygen and Ta/Fe during or after implantation. Firstly, oxygen diffusion may occur along with the ion implantation process because of the non-ultra-high vacuum conditions [21, 22]. Secondly, oxygen in air may react with Ta or Fe when the implanted samples were taken out from the ion implantation equipment.

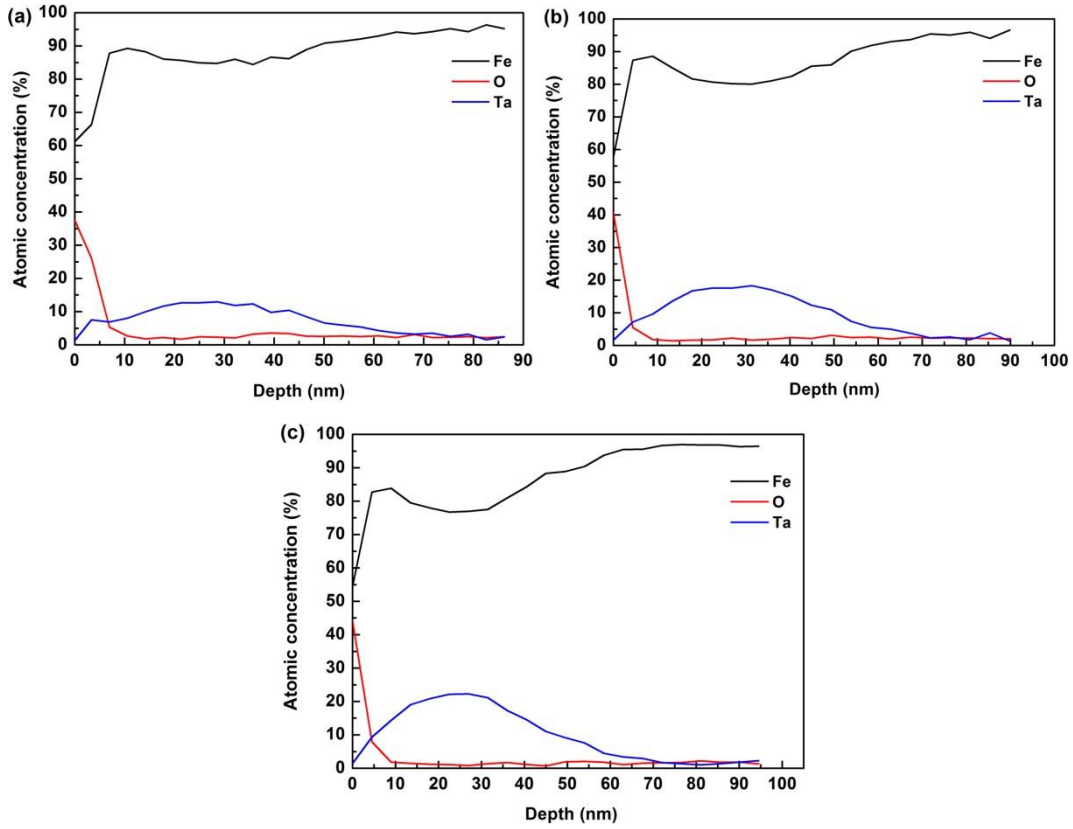

Fig. 2AES depth profiles of(a) Ta-Fe-5, (b) Ta-Fe-10 and (c) Ta-Fe-30 samples

Fig. 3 presents the potentiodynamic polarization curves of the pure Fe before and after Ta ion

implantation in the SBF at 37 °C. The corresponding electrochemical parameters of corrosion potential (E_{corr}) and corrosion current density (i_{corr}) are listed in Table 2. It is known that value of the E_{corr} is a thermodynamic indication of the corrosion resistance on the surface, and a higher E_{corr} value represents a higher anti-corrosion ability. Whereas the value of the i_{corr} is a kinetic parameter to quantify the corrosion rate and a larger i_{corr} value refers to a higher corrosion rate. As reported in literature [23-25], various values of the E_{corr} were obtained after ion implantation, which were between those of the implanted metal and the substrate. For example, implantation of Zn in the form of metallic state increases the E_{corr} value of a pure Mg substrate [25]. Accordingly, the E_{corr} values of the pure Fe (-0.664±0.016 V/SCE) could be increased by implanting Ta to achieve a higher corrosion potential. It is noted that the i_{corr} value of the pure Fe ($2.26\pm0.84 \times 10^{-6}$ A·cm^{-2}) was increased after Ta ion implantation with relatively lower incident doses, e.g. 5 or 10×10^{16} ions/cm^2. The largest corrosion rate was obtained in the Ta-Fe-5 sample (with a dose of 5×10^{16} ions/cm^2), which is attributed to the combined effects of surface microstructures and roughness. As indicated from the AFM and AES results, a heterogeneous microstructure of the Ta/Fe oxides was formed on the surface of Ta-Fe-5 sample. The formation of iron oxide on the surface is a possible reason for the accelerated corrosion because of its poor corrosion resistance. The different corrosion potentials between the Ta/Fe oxides and metallic Fe may accelerate the corrosion rate through galvanic corrosion. Furthermore, a rougher surface tends to develop concentrated microscale corrosion cells and thus increase the corrosion rate [26].

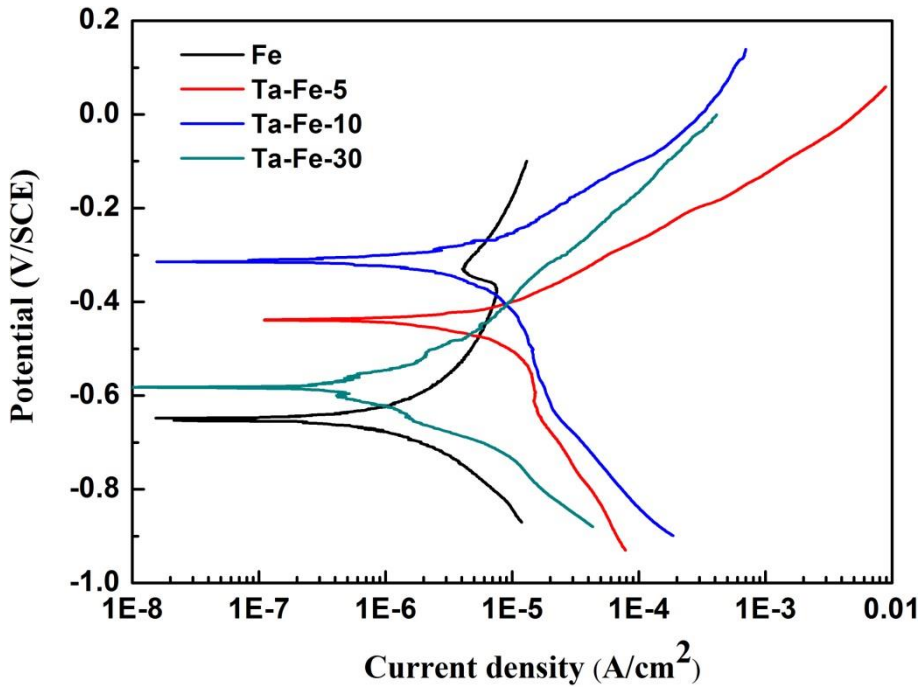

Fig.3 Potentiodynamic polarization curves of pure Fe and Ta-Fe samples in SBFat 37 °C

Table 2 Electrochemical parameters of E_{corr} and i_{corr} of pure Fe and Ta-Fe samples fitted from the potentiodynamic polarization curves

Samples	Fe	Ta-Fe-5	Ta-Fe-10	Ta-Fe-30
E_{corr} (V/SCE)	-0.664±0.016	-0.429±0.010	-0.365±0.050	-0.565±0.017
i_{corr} ($\times 10^{-6}$ A·cm^{-2})	2.26±0.84	7.57±0.24	4.54±1.54	1.71±0.70

Fig. 4 presents the SEM morphologies of the corroded surfaces of the pure Fe and Ta-Fe samples after immersion tests in the SBF at 37ºC for 20 days. In Fig. 4a, the surface of pure Fe is uniformly corroded in the SBF, as indicated by the clear grain boundaries and needle-like corroded morphology in the grains. It is seen from Figs. 4b and 4c that a much worse corrosion morphology occurs on the surfaces of the Ta-Fe-5 and Ta-Fe-10 samples, as evidenced from the coarse corrosion morphologies and large corrosion pits caused by the severe pitting corrosion. For the Ta-Fe-30 sample, as shown in Fig. 4d, a relatively compact corrosion morphology can be observed on the surface with several small corrosion pits showing up near the grain boundaries. It is noted that the corrosion layers of the pure

Fe and Ta-Fe samples are easily exfoliated from the surface by washing with water, leaving the exposure of Fe substrate without the coverage of corrosion products. The results of immersion tests are well consistent with those of the polarization tests, indicating that the corrosion rate of the Fe has been accelerated after the Ta implantation (i.e., samples of Ta-Fe-5 and Ta-Fe-10) due to the enhanced pitting corrosion. It is believed to be beneficial to the biodegradable performance of the Fe in practical application.

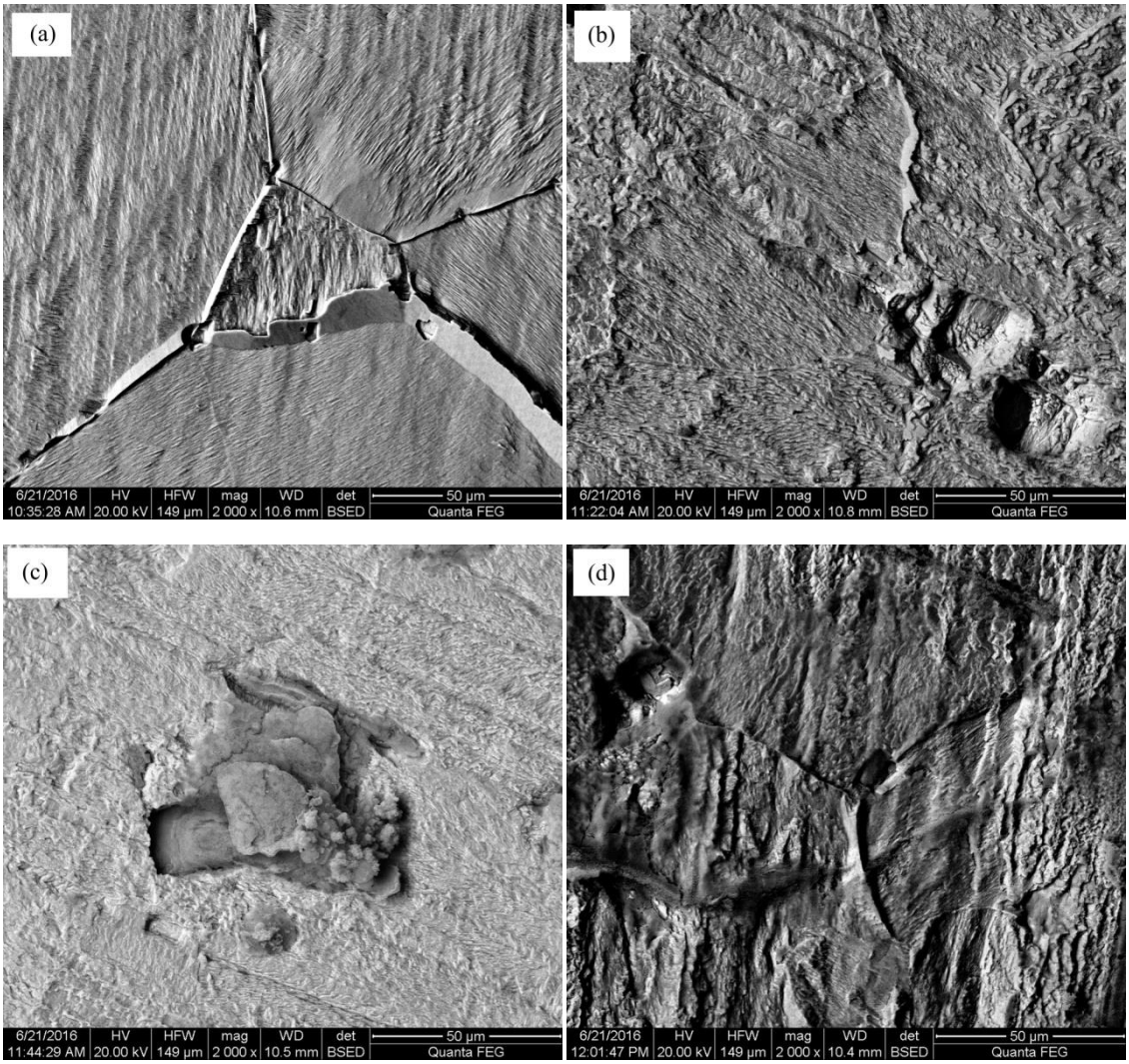

Fig.4 The corroded morphologies of (a) pure Fe, (b) Ta-Fe-5, (c) Ta-Fe-10 and (d) Ta-Fe-30 samples after immersion tests in SBF at 37 ^{o}C for 20 days.

The SEM morphologies of MC3T3-E1 cells on the surfaces of the pure Fe and Ta-Fe samples

after 24-hour culture are shown in Fig. 5. It is seen in Fig. 5a that some osteoblasts spread on the surface of pure Fe and are covered by corrosion products. As seen in Figs.5b, c and d, a significant improvement in cytocompatibility is obtained in the Ta-Fe samples, as evidenced from much larger size and more numbers of osteoblasts adhered. These cells are elongated and show distinctive cell-to-cell attachment with connections with filopodia. They are also found to form a layer-to-layer structure through overlapping on the surfaces. This result indicated that the implanted Ta is beneficial to the proliferation and osseointegration of cells on the pure Fe as it has previously been exhibited on the surface modifications of the other biomaterials, such as NiTi [11, 12, 17] and Co-Cr alloys [27]. In addition, the increased O content on the surface can also enhance the adhesion and proliferation of cells on the surface of implanted samples.

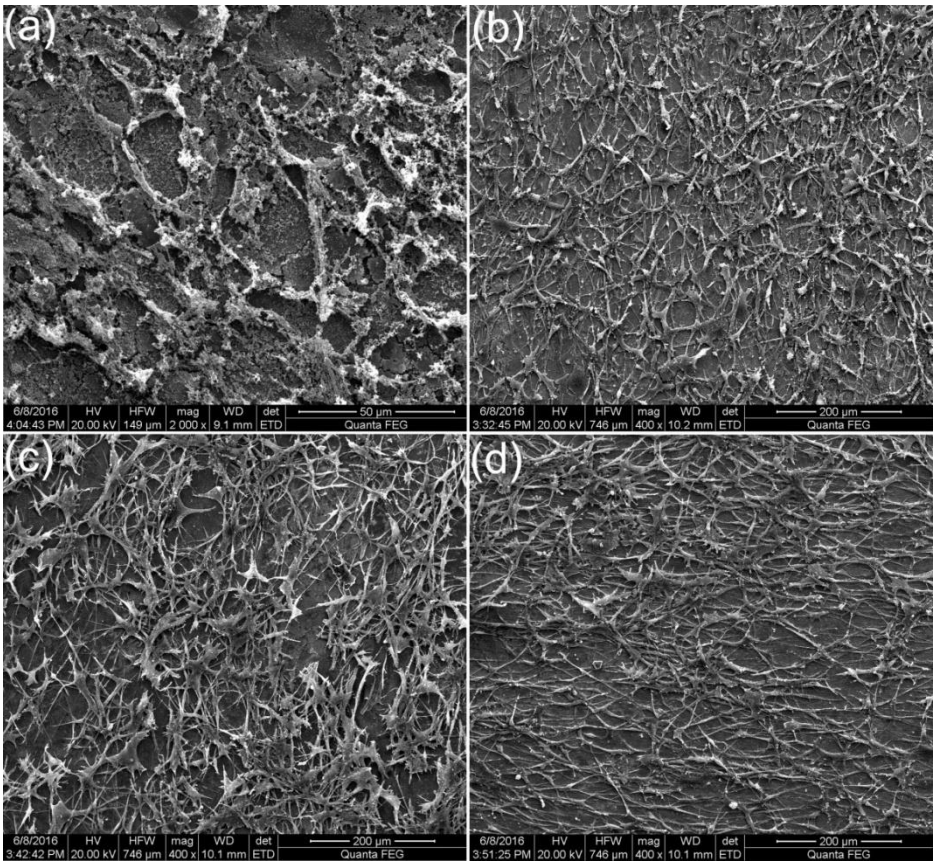

Fig.5 SEM images showing the morphologies of the adherent MC3T3-E1 cells on the surface of (a) pure Fe, (b) Ta-Fe-5, (c) Ta-Fe-10 and (d) Ta-Fe-30 samples after 24 h culture

4. Conclusions

Ta ion implantation has been performed on the surface of the pure Fe to improve its corrosion behavior and cytocompatibility. The results showed that Ta/Fe oxides mixtures were formed on the outmost surface of modified layer with a thickness of 60-80 nm after the Ta ion implantation. The pure Fe modified by the Ta ion implantation exhibited a higher corrosion rate due to the formation of severe pitting corrosion. The MC3T3-E1 cells showed an enhanced adhesion and proliferation behavior on the surfaces of Ta implanted Fe. This study suggested that the Ta ion implantation is an effective method to improve the corrosion behavior and cytocompatibility of the pure Fe for biomedical applications.

Acknowledgment

This work is supported by the National Natural Science Foundation of China (NSFC, No. 51431002).

References

[1] Y.F. Zheng, X.N. Gu, F. Witte, Biodegradable metals, Mater. Sci. Eng. R 77 (2014) 1-34.

[2] E.L. Zhang, H.Y. Chen, F. Shen, Biocorrosion properties and blood and cell compatibility of pure iron as a biodegradable biomaterial, J. Mater. Sci. Mater. Med. 21 (7) (2010) 2151-2163.

[3] M. Schinhammer, A.C. Hänzi, J.F. Löffler, P.J. Uggowitzer, Design strategy for biodegradable Fe-based alloys for medical applications, Acta Biomater. 6 (5) (2010) 1705-1713.

[4] H. Tao, C. Jian, B. Dong, Y. F. Zheng, Fe-Au and Fe-Ag composites as candidates for biodegradable stent materials. J. Biomed. Mater. Res.104B (2) (2016) 225-240.

[5] N.B. Sing, A. Mostavan, E. Hamzah, D. Mantovani, H.Hermawan, Degradation behavior of

biodegradable Fe35Mn alloy stents, J. Biomed. Mater. Res. 103B (3) (2015) 572-577.

[6] T. Kraus, F. Moszner, S. Fischerauer, M. Fiedler, E. Martinelli, J. Eichler, F. Witte, E. Willbold, M. Schinhammer, M. Meischel, P.J. Uggowitzer, J.F. Löffler, A. Weinberg, Biodegradable Fe-based alloys for use in osteosynthesis: Outcome of an in vivo study after 52 weeks, Acta Biomater. 10 (7) (2014) 3346-3353.

[7] W.Q. Wang, J. Wang, M. Qi, Microstructure and in vitro biodegradable properties of Fe-Zn alloys prepared by electroforming, Adv. Mater. Res.1033-1034 (2014) 1200-1206.

[8] M. Peuster, P.Wohlsein, M. Brügmann, M. Ehlerding, K.Seidler, C.Fink, H. Brauer, A. Fischer, G. Hausdorf, A novel approach to temporary stenting: degradable cardiovascular stents produced from corrodible metal - results 6-18 months after implantation into New Zealand white rabbits, Heart 86 (5) (2001) 563-569.

[9] R. Waksman, R. Pakala, R. Baffour, R. Seabron, D. Hellinga, F.O. Tio, Short-term effects of biocorrodible iron stents in porcine coronary arteries, J. Interv. Cardio. 21 (1) (2008) 15-20.

[10] M. Peuster, C. Hesse, T. Schloo, C. Fink, P. Beerbaum, C.V. Schnakenburg, Long-term biocompatibility of a corrodible peripheral iron stent in the porcine descending aorta, Biomaterials 27 (28) (2006) 4955-4962.

[11] T.T. Zhao, R. Yang, C. Zhong, Y. Li, Y.Xiang, Effective inhibition of nickel release by tantalum-implanted TiNi alloy and its cyto-compatibility evaluation in vitro, J. Mater. Sci. 46 (8) (2011) 2529-2535.

[12] Y. Li, T.T. Zhao, S. Wei, Y. Xiang,H. Chen, Effect of Ta_2O_5/TiO_2 thin film on mechanical properties, corrosion and cell behavior of the NiTi alloy implanted with tantalum, Mater. Sci. Eng. C 30 (8) (2010) 1227-1235.

[13] Y. Zheng, Y. Li, J.H. Chen, Z.Y. Zou, Surface characteristics and corrosion resistance of biodegradable magnesium alloy ZK60 modified by Fe ion implantation and deposition, Prog. Nat. Sci. Mater. 24 (5) (2014) 547-553.

[14] T. Huang, Y. Cheng, Y.F. Zheng,In vitro studies on silver implanted pure iron by metal vapor vacuum arc technique, Colloids Surf. B 142 (2016) 20-29.

[15] F.L. Nie, Y.F. Zheng, Y. Wang, J.T. Wang, Microstructures, mechanical behavior, cellular response, and hemocompatibility of bulk ultrafine-grained pure tantalum, J. Biomed. Mater. Res. B 102 (2) (2014) 221-230

[16] Y.D. Liu, C.Y. Bao, D. Wismeijer, G. Wu, The physicochemical/biological properties of porous tantalum and the potential surface modification techniques to improve its clinical application in dental implantology, Mater. Sci. Eng. C 49 (2015) 323-329

[17] C. Park, S.W. Kim, H.E. Kim, T.S. Jang,Mechanically stable tantalum coating on a nano-roughened NiTi stent for enhanced radiopacity and biocompatibility, Surf. Coat. Tech. 305 (2016) 139-145

[18] S.Y. Zhang, Y. Zheng, L.M. Zhang,Y.Z. Bi, J.Y. Li, J. Liu, Y. B. Yu, H.Q. Guo, Y. Li, In vitro and in vivo corrosion and histocompatibility of pure Mg and aMg-6Zn alloy as urinary implants in rat model, Mater. Sci. Eng. C 68 (2016) 414-422.

[19] American Society for Testing and MaterialsASTM-G31-72: standard practice for laboratory immersion corrosion testing of metals, Annual Book of ASTM Standards, ASTM, 2004.

[20] A. Anders, Handbook of Plasma Immersion Ion Implantation and Deposition, John Wiley & Sons, (2000) 1-760.

[21] T.T. Zhao, Y.Li, Y. Xiang, X.Q.Zhao, T.Zhang, Surface characteristics, nano-indentation and

corrosion behavior of Nb implanted NiTi alloy, Surf. Coat. Technol. 205 (19) (2011) 4404-4410.

[22] T.T. Zhao, Y. Li, X.Q.Zhao, H. Chen, T. Zhang, Ni ion release, osteoblasts-materials interactions and hemocompatibility of hafnium implanted NiTi alloy, J. Biomed. Mater. Res.100B (3) (2012) 646-659.

[23] L.H. Mao, Y.L. Wang, Y.Z. Wan, F. He, Y. Huang, Corrosion resistance of Ag-ion implanted Mg-Ca-Zn alloys in SBF, Rare Metal Mater. Eng. 39 (12) (2010) 2075-2078.

[24] X.M. Wang, X.Q. Zeng, G.S. Wu, S.S. Yao, Y.J. Lai, Effects of tantalum ion implantation on the corrosion behavior of AZ31 magnesium alloys, J. Alloy. Comp. 437 (1-2) (2007) 87-92.

[25] G.S. Wu, L. Gong, K. Feng, S.L. Wu, Y. Zhao, P. K.Chu, Rapid degradation of biomedical magnesium induced by zinc ion implantation, Mater. Lett. 65(4) (2011) 661-663.

[26] T.L. Nguyen, A. Blanquet, M.P. Staiger, G.J. Dias, T.B.F. Woodfield, On the role of surface roughness in the corrosion of pure magnesium in vitro, J. Biomed. Mater. Res. 100B (5) (2012)1310-1318.

[27] V.H. Pham, S.H. Lee, Y.L. Li, H.E. Kim, K.H. Shin, Y.H. Koh, Utility of tantalum (Ta) coating to improve surface hardness in vitro bioactivity and biocompatibility of Co-Cr, Thin Solid Films, 536 (2013) 269-274.

Figure Captions:

Fig. 1 AFM images and average surface roughness (Ra) of (a) pure Fe, (b) Ta-Fe-5, (c) Ta-Fe-10 and (d) Ta-Fe-30 samples

Fig. 2 AES depth profiles of(a) Ta-Fe-5, (b) Ta-Fe-10 and (c) Ta-Fe-30 samples

Fig.3 Potentiodynamic polarization curves of pure Fe and Ta-Fe samples in SBF at 37 °C

Fig.4 The corroded morphologies of (a) pure Fe, (b) Ta-Fe-5, (c) Ta-Fe-10 and (d) Ta-Fe-30 samples after immersion tests in SBF at 37 ºC for 20 d.

Fig.5 SEM images showing the morphologies of the adherent MC3T3-E1 cells on the surface of (a) pure Fe, (b) Ta-Fe-5, (c) Ta-Fe-10 and (d) Ta-Fe-30 samples after 24 h culture